BIOCHEMISTRY

 Volume 44, Number 12 March 29, 2005

Articles

Crystal Structure of a Hyperthermophilic Archaeal Acylphosphatase from *Pyrococcus horikoshii*—Structural Insights into Enzymatic Catalysis, Thermostability, and Dimerization[†,‡]

Yuk-Yin Cheung,[§,||] Sonia Y. Lam,[§,||] Wai-Kit Chu,[⊥] Mark D. Allen,[#] Mark Bycroft,[#] and Kam-Bo Wong*[,§]

Department of Biochemistry and Molecular Biotechnology Programme, The Chinese University of Hong Kong, Hong Kong, China, and MRC Centre for Protein Engineering, Hills Road, Cambridge CB2 2QH, United Kingdom

Received October 8, 2004; Revised Manuscript Received January 24, 2005

ABSTRACT: Acylphosphatases catalyze the hydrolysis of the carboxyl−phosphate bond in acyl phosphates. Although acylphosphatase-like sequences are found in all three domains of life, no structure of acylphosphatase has been reported for bacteria and archaea so far. Here, we report the characterization of enzymatic activities and crystal structure of an archaeal acylphosphatase. A putative acylphosphatase gene (PhAcP) was cloned from the genomic DNA of *Pyrococcus horikoshii* and was expressed in *Escherichia coli*. Enzymatic parameters of the recombinant PhAcP were measured using benzoyl phosphate as the substrate. Our data suggest that, while PhAcP is less efficient than other mammalian homologues at 25 °C, the thermophilic enzyme is fully active at the optimal growth temperature (98 °C) of *P. horikoshii*. PhAcP is extremely stable; its apparent melting temperature was 111.5 °C and free energy of unfolding at 25 °C was 54 kJ mol^{-1}. The 1.5 Å crystal structure of PhAcP adopts an α/β sandwich fold that is common to other acylphosphatases. PhAcP forms a dimer in the crystal structure via antiparallel association of strand 4. Structural comparison to mesophilic acylphosphatases reveals significant differences in the conformation of the L5 loop connecting strands 4 and 5. The extreme thermostability of PhAcP can be attributed to an extensive ion-pair network consisting of 13 charge residues on the β sheet of the protein. The reduced catalytic efficiency of PhAcP at 25 °C may be due to a less flexible active-site residue, Arg20, which forms a salt bridge to the C-terminal carboxyl group. New insights into catalysis were gained by docking acetyl phosphate to the active site of PhAcP.

Acylphosphatase (AcP;[1] E.C. 3.6.1.7) is one of the smallest enzymes (∼100 residues) that catalyzes the hydrolysis of the carboxyl−phosphate bond. Its substrates include acetyl phosphate, 1,3-bisphosphoglycerate, succinoyl phosphate,

[†] This work was partially supported by a Strategic Grant (SRP0102) from the Chinese University of Hong Kong.

[‡] The atomic coordinates and structure factors (PDB code 1W2I) have been deposited in the Protein Data Bank, Research Collaboratory for Structural Bioinformatics, Rutgers University, New Brunswick, NJ (http://www.rcsb.org/).

* To whom correspondence should be addressed: Room 507B Mong Man Wai Building, Department of Biochemistry and Molecular Biotechnology Programme, The Chinese University of Hong Kong, Hong Kong, China. E-mail: kbwong@cuhk.edu.hk. Telephone: (852) 2609-8024. Fax: (852) 2603-5123.

[§] Department of Biochemistry, The Chinese University of Hong Kong.

[||] These authors contributed equally to the study.

[⊥] Molecular Biotechnology Programme, The Chinese University of Hong Kong.

[#] MRC Centre for Protein Engineering.

[1] Abbreviations: AcP, acylphosphatase; PhAcP, acylphosphatase from *Pyrococcus horikoshii*; SsoAcP, acylphosphatase from *Sulfolobus solfataricus*; CT, common type; MT, muscle type; AcP-HypF, acylphosphatase domain of hydrogenase maturation factor F; rmsd, root-mean-square deviation; T_m, melting temperature.

10.1021/bi047832k CCC: $30.25
Published on Web 03/01/2005

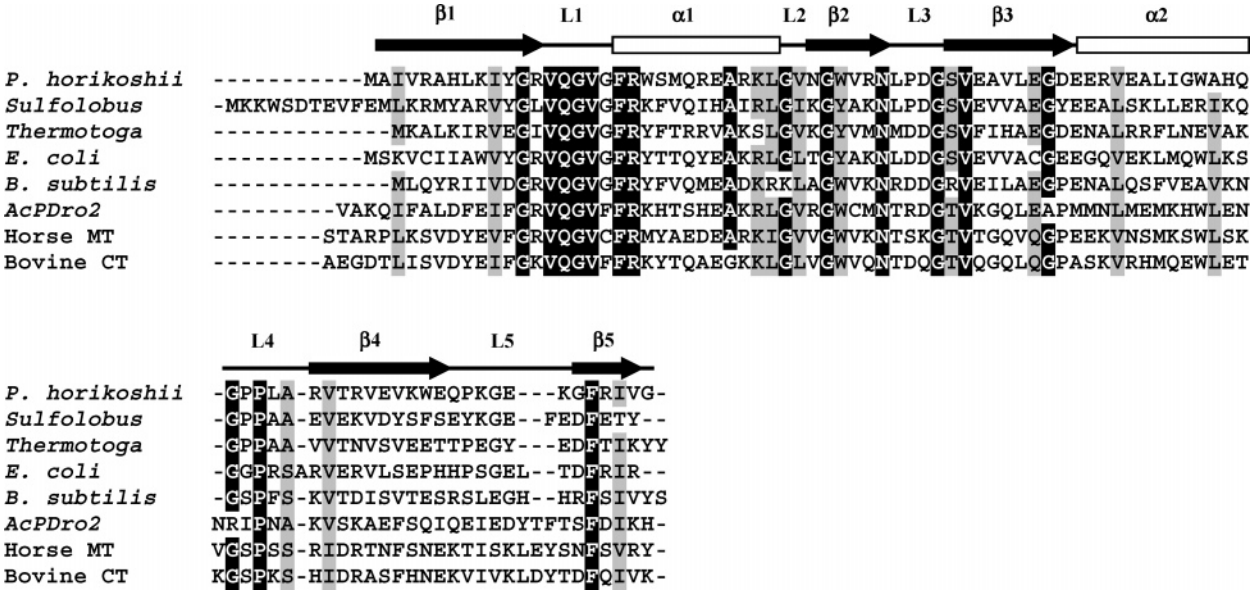

FIGURE 1: Sequence alignment of AcPs. Sequences from *P. horikoshii*, *S. solfataricus*, *Thermotoga maritima*, *E. coli*, *Bacillus subtilis*, fruit fly (AcpDro2), horse (MT), and cow (CT) were aligned by CLUSTALW (*75*), and the alignment was then adjusted manually. Secondary-structure elements of PhAcP were shown above the sequences.

and carbamoyl phosphate, which are intermediates in glycolysis, tricarboxylic acid cycle, pyrimidine, and urea biosynthesis (*1*). Recently, AcP was shown to cleave, albeit at a slower rate, the phosphodiester bond of nucleoside diphosphate and nucleoside triphosphate (*2*). The enzyme was shown to increase the rate of glycolysis. It hydrolyzes 1,3-bisphosphoglycerate to 3-phosphoglycerate and thereby uncouples the ATP-generating reaction catalyzed by phosphoglycerate kinase (*3*−*6*). This regulatory role of AcP on glycolysis is further supported by the fact that the enzyme is overexpressed in tissues that are very active in glycolysis (e.g., brain, heart, and skeletal muscle) (*1*). AcP can also hydrolyze the β-aspartyl phosphate intermediate of the Ca^{2+}- and Na^+,K^+-ATPases and may play a role in regulating ion-transport across the membrane (*7*−*11*).

Two isoforms of AcPs are found in mammalian tissues: muscle-type (MT) AcP is found in skeletal muscle and heart, whereas common-type (CT) AcP is found in erythrocytes, brain, and testis (*1*). AcP has also been isolated and characterized from other higher eukaryotic species such as birds, fish, and fruit flies (*1*, *12*−*14*). The solution structure of horse MT-AcP and crystal structures of bovine CT-AcP and an AcP from *Drosophila* have been reported (*15*−*17*). On the basis of sequence similarity search, AcP-like sequences are found in all three domains (eukarya, bacteria, and archaea) of living organisms (Figure 1). In this study, we have cloned a putative AcP gene from the *Pyrococcus horikoshii* genome (PH0305a) and expressed it in *Escherichia coli*. *P. horikoshii* is a hyperthermophilic archaeon isolated from a hydrothermal vent (*18*). Although PhAcP is extremely thermostable (with a melting temperature of 111.5 °C), its k_{cat} value measured at 25 °C was much smaller than those of other mammalian AcP. To understand the structural basis of thermostability and reduced catalytic efficiency, we have determined the crystal structure of PhAcP to a resolution of 1.5 Å. We have found that the reduced catalytic efficiency of PhAcP at 25 °C is probably a result of a more rigid active site, which is stabilized by extra charge−charge interactions. Another interesting observation is that although PhAcP exists as a monomer in solution, the protein forms a dimer in the crystal structure via antiparallel association of strand 4. On the basis of this first crystal structure of an archaeal AcP, the implications for enzymatic catalysis, thermostability, and dimerization are discussed.

MATERIALS AND METHODS

Structure Determination. Protein expression, purification, and crystallization were performed as described (*19*). Crystals for diffraction data collection were grown by mixing 2 μL of 24 mg/mL protein sample with 2 μL of reservoir solution containing 1.4 M sodium formate and 0.1 M MES at pH 6.0 using the sitting-drop-vapor-diffusion method. Hexagonal crystals (0.3 × 0.3 × 1.0 mm) grew in 2 days at 17 °C. The crystals were cryoprotected by soaking crystals in reservoir solution containing 20% (v/v) glycerol for 1 min at room temperature and were then loop-mounted and flash-cooled in liquid nitrogen. X-ray diffraction data were collected at a wavelength of 0.977 Å at beamline 14.1 of Daresbury Synchrotron Radiation Source at 100 K. A total of 168 frames were recorded with an oscillation angle of 1.0°. Data were processed with MOSFLM, SCALA, and TRUNCATE in the CCP4 suite (*20*) (Table 1). The initial phases of the model were determined by molecular replacement using MOLREP (*21*) in the CCP4 suite using the bovine CT AcP (2ACY) as the search model. Simulated annealing protocols with torsional molecular dynamics implemented in CNS (*22*) were used in the initial refinement cycles. Model building was performed with XTALVIEW (*23*) guided by σ_A-weighted maps (*24*) with $2F_o - F_c$ and $F_o - F_c$ coefficients. Water molecules were located in the $F_o - F_c$ map with peaks of density $>3.0\sigma$. Only water molecules that can form hydrogen bonds to other protein or water atoms were kept. After several rounds of refinement in CNS (R_{cryst} = 19.0%, and R_{free} = 19.8%), REFMAC 5 (*25*) was used for further refinement. At this stage, alternate conformations were introduced to explain the side-chain electron density for 19 residues (I3, K9, R13, E26, L48, D51, E52, R54, K82, and R88 of chain A and K9, S22, E26, L48, D51, R54, R70,

Table 1: Crystallographic Data and Refinement Statistics

diffraction data (values in parentheses are for the highest resolution shell 1.58−1.50 Å)	
space group	$P3_221$
unit cell dimensions [*a*, *b*, and *c* (Å)]	85.34, 85.34, 75.65
resolution range	16.95−1.50
temperature (K)	100
number of measurement	499 655
number of unique reflection	51 268
redundancy	9.7 (9.2)
completeness (%)	99.9 (99.9)
R_{merge}[a] (%)	7.5 (37.2)
mean $I/\sigma(I)$	22.5 (5.2)
refinement	
R_{cryst}[b] (%)	16.6
R_{free}[c] (%)	17.4
model	
number of protein atoms	1526
number of water atoms	209
number of formate atoms	12
mean *B* value (Å^2)	13.8
rmsd from ideal values	
bond distance (Å)	0.01
bond angles (deg)	1.20
Ramachandran plot analysis	
most favored region (%)	92.5
additional allowed region (%)	7.5
other regions (%)	0.0

[a] $R_{merge} = \sum_{hkl}\sum_n|I(hkl)_n - \langle I(hkl)\rangle|/\sum_{hkl}\sum_n I(hkl)_n$, where $I(hkl)_n$ is the observed intensity of the *n*th reflection and $\langle I(hkl)_n\rangle$ is the mean intensity of reflection *hkl*. [b] $R_{cryst} = \sum||F_o| - |F_c||/\sum|F_o|$, where F_o and F_c are the observed and calculated amplitudes, respectively. [c] The free set contains 2601 (5.1% of the total) reflections.

R73, and Q80 of chain B), and hydrogen atoms were added in the riding positions. The final model has an R_{cryst} of 16.6% and an R_{free} of 17.4% and is of good quality as tested by PROCHECK (*26*). The statistics for diffraction data and structure refinement are summarized in Table 1.

Enzyme Assay. AcP activity was measured using a continuous optical assay with benzoyl phosphate as the substrate (*27*). Benzoyl phosphate was synthesized as described (*28*). To measure the pH optimum of PhAcP, 1 mM of substrate was incubated with 10 nM of PhAcP at 25 °C in 0.1 M sodium acetate buffer at pH 3.5, 4.0, 5.0, 5.3, 5.5, 5.7, 5.9, or 0.1 M MES buffer at pH 6.0, 6.2, 6.5, or 6.7, or 0.1 M HEPES buffer at pH 7.0, 7.2, 7.5, 7.7, or 50 mM Tris buffer at pH 8.0, 8.5, or 9.0. The rate of hydrolysis, monitored by the decrease of the absorbance at 283 nm, was the highest at pH 5.3. Therefore, we chose to determine the kinetic parameters at this optimum pH of 5.3. To this end, the substrate was incubated with 7.5, 10, or 12.5 nM of PhAcP at 25, 30, 35, 40, or 45 °C in 0.1 M sodium acetate buffer at pH 5.3, and the rate of hydrolysis was monitored by the decrease of the absorbance at 283 nm. The kinetic parameters, K_m and k_{cat}, were determined by measuring the initial rates at substrate concentration ranging from 0.05 to 1.0 mM and fitting the data to the Michaelis−Menton equation by nonlinear regression. Protein concentration was determined by absorbance at 280 nm using an extinction coefficient of 24 040 M^{-1} cm^{-1}.

Guanidine-Induced Denaturation. Protein samples (25 μM) were equilibrated with 0−7.2 M of guanidine hydrochloride (GdnHCl) in 10 mM sodium phosphate buffer at pH 7.4 and 25 °C for 30 min before circular dichroism measurement. GdnHCl was used because urea cannot denature PhAcP completely. The concentration of GdnHCl solution was determined by refractive index measurement as described (*29*). The unfolding of PhAcP was monitored by molar ellipticity at 222 nm at 25 °C using a 1-mm pathlength cuvette with a JASCO J810 spectropolarimeter equipped with a peltier-type temperature control unit. Reversibility of denaturation was checked by diluting a guanidine-denatured sample and found to be >99% reversible. The data were fitted by nonlinear regression to a two-state model, and the free energy of unfolding without denaturant, $\Delta G_{(H_2O)}$, was obtained by the linear extrapolation model (*30*).

Differential Scanning Calorimetry. Melting temperature of PhAcP was determined by differential scanning calorimetry with Nano-DSC III from Calorimetry Sciences Corporation (Lindon, Utah). Protein samples (50 μM) were dialyzed against 10 mM sodium phosphate buffer at pH 7.4 and degassed thoroughly before loading to the sample cell. The dialysis buffer was loaded to the reference cell. Baseline scans were obtained by filling dialysis buffer to both cells. Temperature was scanned from 25 to 130 °C at a rate of 1 °C/min. Rescanning of the samples indicated that the thermal denaturation of PhAcP was irreversible. An apparent melting temperature was estimated by the midpoint of thermal transition.

Docking Simulation. Docking of acetyl phosphate to PhAcP was performed using AUTODOCK 3.0.5 (*31*). The target structure contained all protein atoms in chain A and a bound water (Wat48Z) in the active-site pocket of PhAcP. Polar hydrogen atoms were then added to the target structure. The ligand structure of acetyl phosphate was constructed using the PRODRG2 server (*32*). A mass-centered grid map was constructed with a dimension of 60 × 60 × 60 points and a spacing of 0.375 Å. A total of 50 runs were performed with Lamarckian genetic algorithm using default parameters. The docked conformations of acetyl phosphate were then clustered and sorted by energy.

RESULTS AND DISCUSSION

Recombinant PhAcP Is Active. In the genome of a hyperthermophilic archaeon, *P. horikoshii*, the gene PH0305a has been annotated as a putative AcP (*33*). We have cloned and overexpressed the gene in *E. coli*. AcP from *P. horikoshii* (PhAcP) shares ~30% sequence identity to other eukaryotic homologues. The molecular weight of the recombinant PhAcP determined by mass spectrometry was 10 128.6 Da, which agrees with the theoretical prediction based on the primary sequence. PhAcP was monomeric in solution as suggested by analytical gel filtration, and the elution volume of PhAcP was similar for protein samples ranging from 0.5 to 20 mg/mL (data not shown).

In this study, we have demonstrated that recombinant PhAcP is active using benzoyl phosphate as the substrate. The pH optimum of PhAcP was pH 5.3 (data not shown), which agrees with the value reported for other AcPs (*13*). At 25 °C, pH 5.3, the K_m and k_{cat} values were 0.12 ± 0.03 mM and 93.5 ± 1.6 s^{-1}, respectively. Table 2 compares the reported values of enzymatic parameters of different AcPs. The K_m value of PhAcP is similar to those of other mesophilic AcPs. On the other hand, the k_{cat} value of PhAcP is higher than that of isoform 1 of *Drosophila* AcP (AcPDro), but is much lower than those of the mammalian homologues and isoform 2 of *Drosophila* AcP (AcPDro2).

Table 2: Enzymatic Parameters of PhAcP and Other Mesophilic AcPs at pH 5.3 and 25 °C Using Benzoyl Phosphate as the Substrate

enzyme	k_{cat} (s^{-1})	K_m (mM)	k_{cat}/K_m (s^{-1}/mM)
PhAcP	93.5	0.12	779
bovine CT-AcP (*40*)	1524	0.11	12 700
human CT-AcP (*13*)	1420	0.15	9470
human MT-AcP (*13*)	1230	0.36	3420
AcPDro (*13*)	35	0.18	194
AcPDro2 (*12*)	735	0.80	920

The temperature dependency of kinetic parameters of PhAcP was studied. The k_{cat} of PhAcP was increased >4-fold by an increase of temperature from 25 to 45 °C. The k_{cat} values of PhAcP at 25, 30, 35, 40, and 45 °C were 93.5, 191, 275, 290, and 467 s^{-1}, respectively. On the other hand, the K_m values remained ~0.12 mM in the temperature range. The Arrhenius plot (ln k_{cat} versus 1/*T*) gave a straight line (Figure 2). By linear extrapolation, the k_{cat} value of PhAcP at 98 °C was estimated to be ~10 000 s^{-1}. Taken together, although PhAcP is a sluggish enzyme at 25 °C, the enzyme should have enough catalytic activities at the optimal growing temperature (98 °C) of *P. horikoshii*.

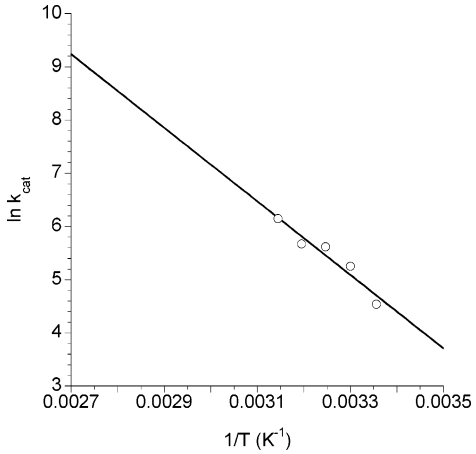

FIGURE 2: Temperature-dependency of k_{cat} values of PhAcP. The k_{cat} values of PhAcP determined at 25, 30, 35, 40, and 45 °C were 93.5, 191, 275, 290, and 467 s^{-1}, respectively. The Arrhenius plot (ln k_{cat} versus 1/*T*) gave a straight line. The k_{cat} value was estimated to be ~10 000 s^{-1} at 98 °C ($1/T = 0.0027$ K^{-1}) by linear extrapolation.

PhAcP Is Extremely Thermal-Stable. Thermal unfolding of PhAcP was monitored by differential scanning calorimetry (Figure 3A). PhAcP started to unfold at ~100 °C, and its apparent melting temperature (T_m) was 111.5 °C. Free energy of unfolding [$\Delta G_{(H_2O)}$] of PhAcP was determined by guanidine-induced denaturation, which followed a reversible and two-state transition (Figure 3B). At 25 °C, the free energy of unfolding, midpoint of transition, and *m* value were 54.4 ± 2.2 kJ mol^{-1}, 4.99 ± 0.01 M, and 10.9 ± 0.4 kJ mol^{-1} M^{-1}, respectively. These data indicate that PhAcP is an extremely stable protein. For comparison, the $\Delta G_{(H_2O)}$ and T_m values are 18.3 kJ mol^{-1} and 53.9 °C for human CT-AcP (*34*) and 28.7 kJ mol^{-1} and 56.6 °C for human MT-AcP (*35*).

Overall Structure. The structure of PhAcP was determined at a resolution of 1.5 Å (R_{cryst} = 16.6%, and R_{free} = 17.4%, see Table 1 for refinement statistics). The final model consists of a dimer of AcP, 209 water molecules, and 4 formate ions.

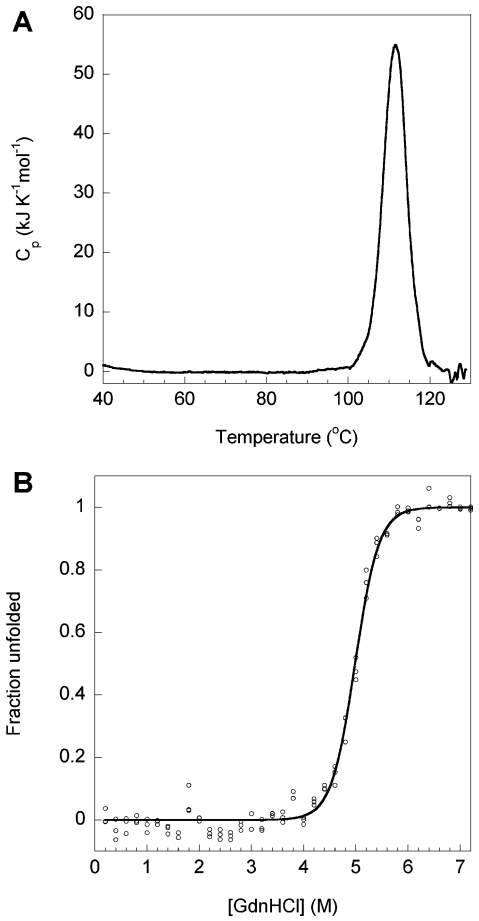

FIGURE 3: PhAcP is extremely stable. (A) Thermal unfolding of PhAcP monitored by differential scanning calorimetry. The apparent melting temperature of PhAcP was 111.5 °C. (B) Equilibrium guanidine-induced denaturation of PhAcP at 25 °C. The unfolding of PhAcP was followed by molar ellipticity at 222 nm, and the raw data were converted to a fraction of the unfolded protein using a two-state model (*30*). The midpoint of transition, *m* value, and free energy of unfolding were 4.99 ± 0.01 M, 10.9 ± 0.4 kJ mol^{-1} M^{-1}, and 54.4 ± 2.2 kJ mol^{-1}, respectively.

The structures of the two PhAcP monomers are essentially identical, with a root-mean-square deviation (rmsd) between Cα atoms of 0.3 Å. PhAcP adopts an α/β sandwich fold, with two antiparallel helices packed on a five-stranded antiparallel β sheet (Figure 4A). The right-handed twisted β sheet follows a 4-1-3-2-5 β-strand topology. The loops connecting the secondary structure elements of PhAcP are labeled L1−L5. There is no loop between strand 3 and helix 2. The L1 loop formed by the consensus sequence $V_{14}QGVGFR_{20}$ creates a cradle-like structure for substrate binding (see below). L2 is a short loop (residues 31−32) connecting helix 1 and strand 2. The backbone N atoms of Gly31 and Val32 form capping hydrogen bonds to the carbonyl group of Ala27. The conformation of L2 is facilitated by the backbone dihedral angles ($\phi = 75°/\psi = 34°$) of the conserved residue Gly31. The sequence stretches $L_{39}PDG_{42}$ and $P_{66}PLA_{69}$ form type-I β turns in L3 and L4, respectively. L5 (residues 80−85), the longest loop in PhAcP, runs across the protein molecule connecting strands 4 and 5.

PhAcP Forms a Dimer in the Crystal Structure. One unique feature of PhAcP is that the protein forms a dimer in the crystal structure. Two monomers of PhAcP bind together

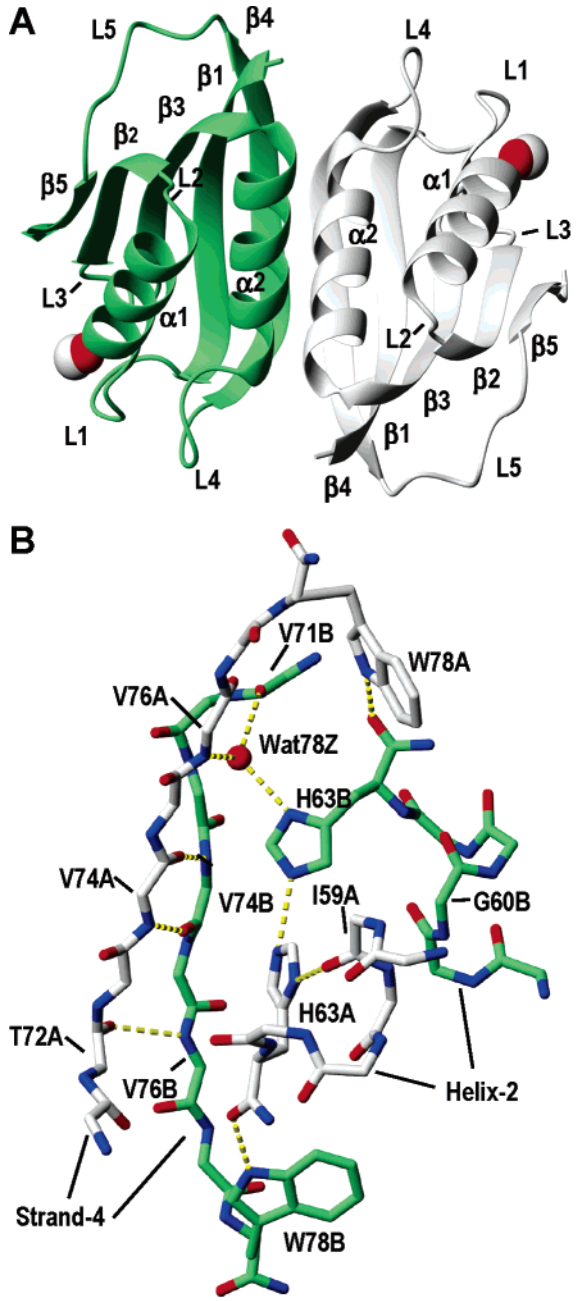

FIGURE 4: PhAcP forms a dimer in the crystal structure. Chain A is color-coded white, while chain B is color-coded green. (A) Ribbon representation of PhAcP. The location of the active sites was indicated by the bound formate ions, which are shown in a space-fill model. The secondary structure elements are labeled. (B) Close-up view of the dimeric interface showing the interchain hydrogen bonds.

via antiparallel association of strand 4, with formation of nine interchain hydrogen bonds (Figure 4B). The dimeric interface among the two AcPs buries 1340 Å^2 of solvent-accessible surface area. Ile59, Gly60, His63, and Val74 become completely buried upon dimerization. Helix 2 of the two monomers packs tightly against each other at an angle of ~75°, with Ile59 in close contact with Gly60 of the opposite monomer. His63 is involved in a network of hydrogen bonds bridging His63 and Trp78 of the two monomers (Figure 4B). Noteworthy, the dimeric interface is not completely symmetrical. For example, the ND1 atom of His63A forms a hydrogen bond to the O atom of Ile59A, while the ND1 atom of His63B forms a hydrogen bond to a

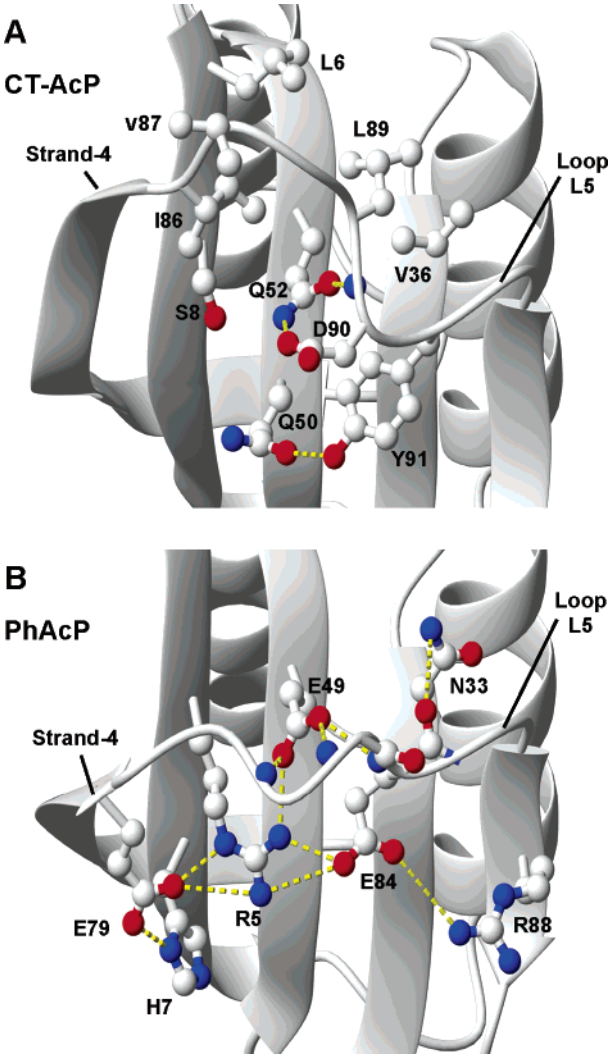

FIGURE 5: Structure of the L5 loop of AcP is not conserved. Residues involved in stabilizing the conformation of the L5 loop of (A) CT-AcP and (B) PhAcP are shown. Hydrogen bonds and salt bridges are represented by dotted lines.

bound water molecule (Wat78Z), which forms hydrogen bonds that bridge Val71B and Val76A (Figure 4B).

The L5 Loop of PhAcP Is Not Conserved. Although PhAcP shares a similar fold to bovine common-type AcP (CT-AcP) (with rmsd of 0.66 Å for Cα atoms of 84 matched residues), large structural differences are observed in the L5 loop. Sequence alignment shows that the region is the least conserved among AcP (Figure 1). Strand 4 of PhAcP is shorter than that of CT-AcP by three residues. In CT-AcP, the L5 is stabilized by hydrophobic interactions involving Leu6, Val36, Ile86, Leu89, and Tyr91 and by hydrogen bonds involving Gln50, Gln52, Asp90, and Tyr91 (Figure 5A). In PhAcP, the L5 is stabilized predominantly by an extensive network of salt bridges and hydrogen bonds: Glu79 forms salt bridges to Arg5 and His7, the backbone amide of Lye82, Gly83, and Glu84 forms hydrogen bonds to Asn33 and Glu49, and Glu84 forms salt bridges to Arg5 and Arg8 (Figure 5B). These extra interactions probably contribute to the thermostability of PhAcP.

Active-Site Structure. The active site is located at the cleft between loop L1 and L3. The residues Val14−Arg20 create a cradle-like conformation, in which backbone N atoms of Gly16, Val17, Gly18, Phe19, and Arg20 are pointing toward

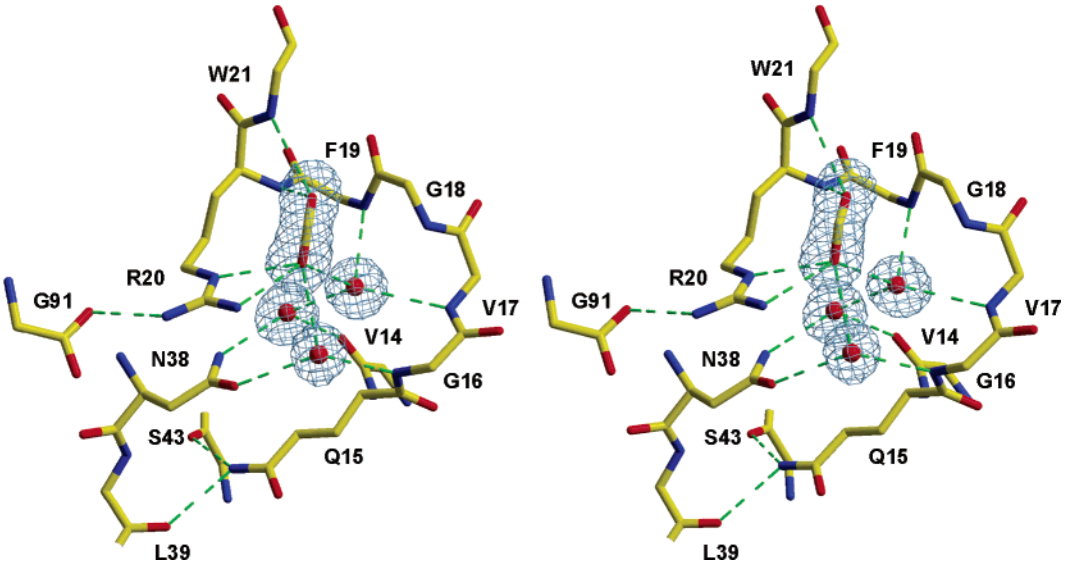

FIGURE 6: Stereodiagram showing the active-site structure of PhAcP. One formate ion and three water molecules were found in the active site. These bound atoms were omitted in calculating the $F_o - F_c$ difference map, which is contoured at 3σ in the figure. Hydrogen bonds are represented by dotted lines.

the center of the cradle (Figure 6). The conformation of L1 loop is maintained by the conserved sequence of V_{14}QGV-FR_{20}. The only variable residue in L1 is Gly18. In bovine CT-AcP, the corresponding residue is Phe21, an exposed residue not involved in stabilization of the L1 loop. The two active sites of the PhAcP dimer are ~40 Å away from each other (Figure 4A), and their structures are similar. Because PhAcP exists as a monomer in solution, dimerization is unlikely to be important for the biological function of the enzyme.

Site-directed mutagenesis and structural studies on mammalian AcP suggest that Arg23 and Asn41 are essential to catalysis (*16*, *36*, *37*). It was proposed that Arg23 binds the phosphate group of the substrate and Asn41 binds an active-site water molecule that serves as the attacking nucleophile for hydrolysis of the carboxyl−phosphate bond (*16*). In PhAcP, the corresponding residues are Arg20 and Asn38. In this study, PhAcP was crystallized with sodium formate. Each active site binds one formate ion and three water molecules (Figure 6). The bound formate ion forms salt bridges to the guanido group of Arg20 and forms hydrogen bonds to the backbone amide of Arg20 and Trp21. In bovine CT-AcP, there is a sulfate ion that occupies the formate-binding site. In PhAcP, the guanido group of Arg20 also forms a salt bridge to the C-terminal carboxyl group (Gly91) of the protein (Figure 6). This salt bridge, not found in CT-AcP, may provide extra interactions to stabilize the side-chain conformation of Arg20.

The side chain of Asn38 of PhAcP is hydrogen-bonded to two water molecules in the active-site cradle (Figure 6). The position of these two water molecules is conserved in CT-AcP. NE2 atom of Gln15 is hydrogen-bonded to the backbone O atoms of Leu39 and Ser43 in the L3 loop. These hydrogen bonds lock the side chain of Gln15 in an extended conformation, which in turn keeps the side chain of Asn38 pointing toward the active-site cradle (Figure 6). In an AcP-like domain of *E. coli* hydrogenase maturation factor HypF (AcP-HypF), which does not have any AcP activities, a one-residue deletion in L3 prevents such hydrogen-bond formation (*38*). As a result, the corresponding Asn residue (residue 41 in AcP-HypF) is in an inactive conformation, pointing away from the active-site cradle. There is a third water molecule in the cradle of PhAcP, which is hydrogen-bonded to backbone amide of Val17 and Phe19. In CT-AcP, the position of this water molecule is occupied by a chloride ion. The three water molecules in the cradle form extensive hydrogen bonds to the bound formate ion, backbone amide of residues in L1, and side chain of Asn38 (Figure 6).

A Model for Enzyme−Substrate Interactions by Docking Simulation. To date, there is no structure of the enzyme−substrate or enzyme−transition-state analogue for AcP available. To yield a better understanding of enzyme−substrate interactions, we have used AUTODOCK 3 (*31*) to dock acetyl phosphate to PhAcP containing a bound water molecule (Wat48Z) in the active-site pocket. It was proposed that the bound water serves as a nucleophile for catalysis. The structure of the docked substrate with the lowest energy is shown in Figure 7B. This enzyme−substrate model is consistent with existing experimental evidence and the mechanism previously proposed (*16*). The bound water is positioned in such a way that its O atom aligns along a straight line with the phosphorus atom and the bridge O atom of acetyl phosphate and is ready for an in-line attack on the phosphate group. Interactions that stabilize the enzyme−substrate complex are summarized in Figure 7C.

Like most uncatalyzed hydrolysis of phosphate monoesters, enzymatic hydrolysis of acyl phosphate is likely to occur via a concerted reaction (*39*). A substrate-assisted catalytic mechanism was proposed by Thunnissen et al. (*16*), which suggests that the phosphate group of the substrate activates the nucleophile water by accepting one of its protons (Figure 7A). Similar to other AcP, there is no residue near the active site of PhAcP that can carry out general acid/base catalysis or serve as a nucleophile. It has been proposed that catalysis is mediated by transition-state stabilization within the active-site cradle (*16*).

Our model of the enzyme−substrate complex provides three new structural insights into the catalytic mechanism of AcP. First, our model predicts that Asn38 contributes to catalysis via enzyme−transition-state complementarity, in

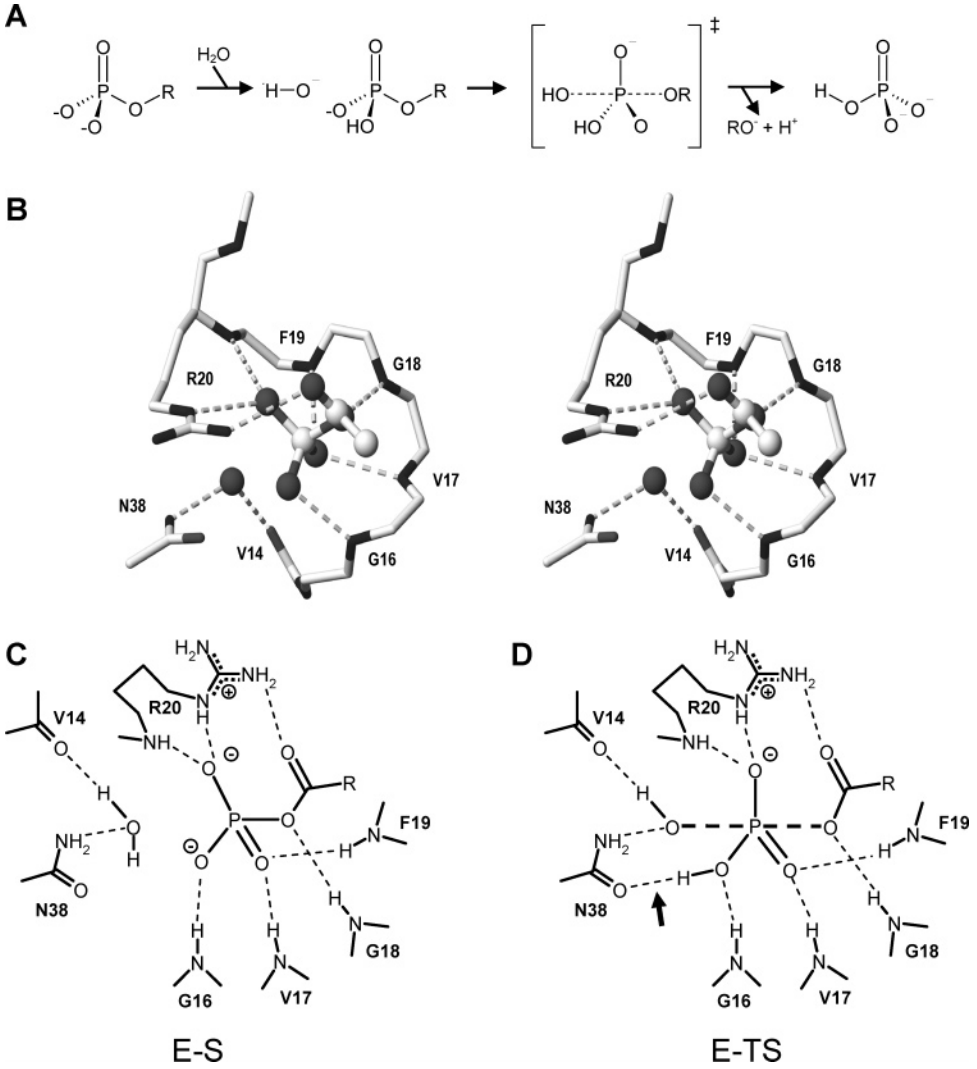

FIGURE 7: Modeling enzyme−substrate interactions in AcP. (A) Substrate-assisted catalytic mechanism proposed by Thunnissen et al. (*16*). (B) Stereodiagram showing the model of the PhAcP−substrate complex. Acetyl phosphate was docked to the active site of PhAcP. The conformation of acetyl phosphate with the lowest energy was shown. Hydrogen bonds are represented by dotted lines. (C and D) Schematic diagrams showing the proposed interactions (thin dotted lines) that stabilize the substrate (C) and transition state (D). The hydrogen bond (indicated by an arrow) between the OD1 atom of Asn38 and the nonbridge O atom of the phosphate group is expected to form only after the phosphate group has been protonated and contribute to catalysis by enzyme−transition-state complementarity.

addition to its generally accepted role of binding a nucleophile water. In our model, Asn38 does not make any interaction with the substrate. The distance between the OD1 atom of Asn38 and the closest nonbridge oxygen atom is ~3.4 Å. However, it is anticipated that, after accepting a proton from the nucleophile water and during formation of the pentacoordinate transition state, the phosphate group will move closer toward the OD1 atom of Asn38, which will then form a hydrogen bond with the protonated nonbridge oxygen atom (Figure 7D). This hydrogen bond, only found in the transition state, contributes to enzymatic catalysis via enzyme−transition-state complementarity. This model is consistent with the findings that mutations at Asn41 (e.g., N41A) of MT-AcP decreased the k_{cat}/K_m value dramatically without affecting the K_m value (*37*). Moreover, our model predicts that stabilization of the transition state requires an asparagine at position 38, which can serve as a hydrogen-bond donor as well as an acceptor (Figure 7D). This is consistent with the observation that a N41D mutant of mammalian AcP has only 1% residual activity (*37*). Taken together, in addition to its role of binding an active-site water, Asn38 also plays a direct role in transition-state stabilization.

Second, the methyl group of acetyl phosphate is pointing away from the active-site cradle and is not making any interactions with the enzyme molecule. This arrangement agrees with the finding that K_m values for different acylphosphate substrates are similar to each other (*40*). Third, our model suggests that Arg20 forms a hydrogen bond to the carbonyl group of the substrate. Such interaction may contribute to the substrate specificity of AcP and may help to stabilize the negative charge developed on the leaving group. Interactions that stabilize the transition state of enzymatic hydrolysis of acyl phosphates are summarized in Figure 7D.

Structural Basis of Hyperthermostability. P. horikoshii is a hyperthermophilic archaeon that grows optimally at 98 °C (*18*). To adapt to this extreme environment, the proteins of the organism must be able to resist denaturation and remain active at temperatures close to the boiling point of water. We have shown that PhAcP is an extremely stable protein.

Table 3: Statistics of Structural Comparison among Homologous AcPs

	ion pair (Å)[a]			hydrogen	buried ASA (Å^2)[c]		
	4	6	8	bond[b]	all	nonpolar	polar
PhAcP							
chain A	6	13	17	84	9358	5487	3870
chain B	6	14	18	78	9459	5541	3919
dimer	12	30	40	168	20 160	11 778	8379
bovine CT	3	4	8	82	9459	5541	3919
horse MT[d]	4	9	14	87	10 076	5911	4165
AcPDro2	3	7	11	77	9408	5514	3895

[a] The criteria of Szilagyi and Zavodszky (*42*) was used to classify ion pairs using three distance limits of 4, 6, and 8 Å. [b] The numbers of hydrogen bonds were determined using HBPLUS (*73*). [c] The solvent-accessible surface area was calculated by NACCESS (Hubbard, S. J. and Thornton, J. M., Department of Biochemistry and Molecular Biology, University College, London, U.K.) using a probe radius of 1.4 Å. Surfaces of N and O atoms were considered polar, whereas the surfaces of other atoms were nonpolar. The buried accessible surface area was calculated by subtracting the surface area calculated for the native state from those calculated for the Ala-X-Ala tripeptide (*74*). [d] The average values for the NMR ensemble are shown.

The differential scanning calorimetry data suggest that the protein remains folded up to ~100 °C, with an apparent melting temperature of 111.5 °C (Figure 3A). In contrast, the melting temperatures of mesophilic AcP are in the range of ~50−60 °C (*34*, *35*).

Structure comparison between pairs of thermophilic and mesophilic proteins has identified a number of structural features that can enhance stability of proteins (*41*−*46*). It is generally agreed that different proteins may use a different combination of features to achieve thermostability (*47*). We have compared the number of ion pairs, number of hydrogen bonds, and accessible surface areas of homologous AcP (Table 3). Our analyses clearly indicate that PhAcP has more ion pairs than other mesophilic homologues. In PhAcP, there is a network of ion pairs consisting of 13 charged residues on the hydrophilic side of the β sheet (Figure 8). In CT-AcP, This ion-pair network is not found in mesophilic CT-AcP, in which 7 of the 13 residues are substituted by polar residues. The network can be divided roughly into two clusters of charged residues. One cluster (R5, E49, K77, E79, E84, and R88), located near the L5 loop, is involved in stabilizing the conformation of the loop (see above). Another cluster (K9, R37, R41, E45, R73, and E75) is located at the bottom of the β sheet. The short distances (<3 Å) between the side-chain atoms of Glu45, Glu79, and His7 suggest that His7 is protonated, which bridges the two clusters by forming hydrogen bonds to both Glu45 and Glu79. It is highly likely that this ion-pair network contributes to the thermostability of PhAcP.

It has been observed that thermophilic proteins tend to have more ion pairs than their mesophilic homologues (*42*). Although it has been argued that electrostatic interactions may not contribute to protein stability because of the large entropic and desolvation penalty of fixing two charged side chains (*48*), recent theoretical calculations suggest that electrostatic interactions should stabilize the protein at high temperatures where the desolvation penalty is less because of the increased thermal motion of water (*49*). Experimentally, the stabilizing role of electrostatic interactions have been reported in many cases (*50*−*57*). The ion-pair network

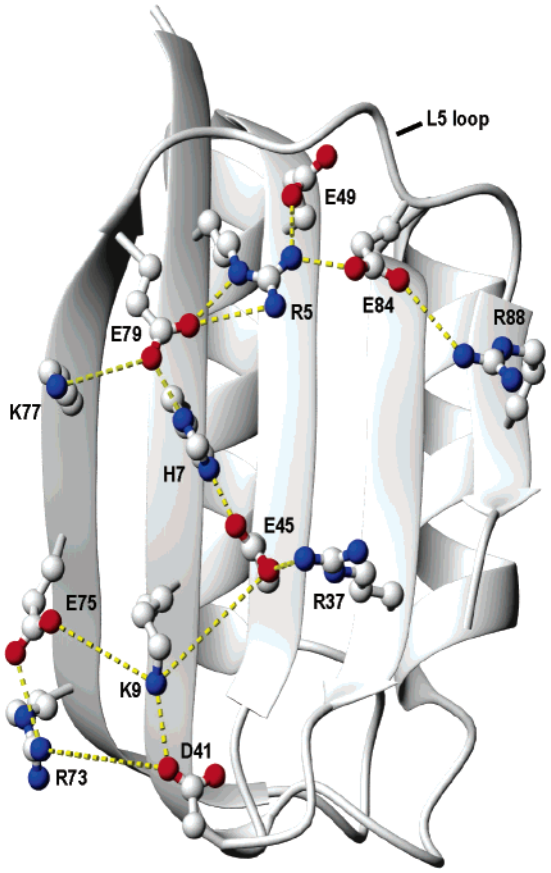

FIGURE 8: Ion-pair network on the β sheet of PhAcP that is absent in mesophilic AcPs.

observed in PhAcP further supports the contribution of electrostatic interactions to the thermostability of proteins.

Another notable feature of PhAcP is that the protein contains more proline residues. Proline residues contribute to protein stability by entropically destabilizing the denatured states (*58*). One proline residue, Pro40, takes the $i + 1$ position of the type I β turn ($L_{39}PDG_{42}$) in L3 loop. Noteworthy, this proline residue is conserved in archaeal AcP but not in bacterial or eukaryotic AcP (Figure 1). It is likely that the proline ring stabilizes the turn structure in L3 and contributes to the thermostability of PhAcP. This β turn is also stabilized by the hydrogen bond between the side chain of Asp41 and backbone amide of Gly42. Noteworthy, Asp41 is conserved in bacterial and archaeal AcP but not in eukaryotic AcP. Two other extra proline residues are located in L4 and L5 loops (Figure 1).

Structural Basis of Reduced Catalytic Efficiency at Ambient Temperatures. In this study, we have shown that PhAcP is less active than other mammalian AcPs at 25 °C (Table 2). There is no change in the structure of the active-site cradle and the side-chain conformation of the active-site residues (Arg20 and Asn38). It is intriguing what factors cause the big differences in catalytic efficiency. Recently, there have been a number of studies comparing the catalytic efficiency of psychrophilic, mesophilic, and thermophilic enzymes (*59*−*63*). Although the activity of thermophilic and mesophilic enzymes is usually comparable at their respective optimal working temperatures, thermophilic enzymes are often less efficient enzymes than the mesophilic and psychrophilic homologues at moderate temperatures. It has been hypoth-

esized that lower catalytic efficiency is due to the active sites of thermophilic enzymes being less flexible (*61*). In PhAcP, the active-site residue Arg20 forms a salt bridge to C-terminal carboxyl group of Gly91 (Figure 6). This salt bridge, not found in mesophilic AcP, may stabilize the active-site structure but at the same time reduce the flexibility of Arg20 and contribute to the reduced catalytic efficiency of PhAcP at 25 °C.

Estimation of the k_{cat} Value of PhAcP at 98 °C. Although PhAcP is not efficient at 25 °C, the enzyme is fully active at the optimal growing temperature of *P. horikoshii*. Experimentally, it is impossible to assay the enzyme activity of PhAcP directly at 98 °C because the uncatalyzed hydrolysis of the acyl-phosphate substrate is too fast at high temperatures to allow an accurate measurement of kinetic parameters. Instead, we measured the kinetic parameters of PhAcP at 25−45 °C and estimated the k_{cat} value of PhAcP at 98 °C by linear extrapolation of the Arrhenius plot (Figure 2). The estimated k_{cat} value of ∼10 000 s^{-1} is reasonable, considering that the measured k_{cat} value increased >4-fold when the temperature increased from 25 to 45 °C, and many chemical reactions double its rate with an increase of ∼10 °C. In comparison with k_{cat} values of other mammalian AcPs (Table 2), PhAcP should have enough catalytic activity for the enzyme to carry out its biological functions at the optimal growing temperature of *P. horikoshii*.

Dimerization of PhAcP. In our study, we have shown that although PhAcP exists as a monomer in solution, it can dimerize via antiparallel association of strand 4. This is the first report of dimeric AcP in the crystal structure. The driving forces of dimerization are the formation of interchain hydrogen bonds and burial of the hydrophobic surface area (∼750 Å^2). The dimeric interface consists of mainly hydrophobic residues (Ile59, Val71, Val74, Val76, and Trp78) from helix 2 and strand 4. The only buried polar residue is His63, which is involved in a hydrogen-bond network in the interface (Figure 4B).

AcPs have been studied extensively as a model for amyloid fibril formation (*64*−*70*). It was shown that AcP can be induced to form *in vitro* amyloid fibrils that closely resemble those observed in clinical cases (*71*). It has been widely accepted that aggregation of amyloid originates from partially unfolded states. For example, mutations that destabilize the native state were shown to promote aggregation by populating the partially unfolded intermediates (*64*−*69*). In a recent study, Chiti and co-workers demonstrated that amyloid formation can originate from "nativelike" states, albeit at a slower rate than that originates from partially unfolded states (*72*). In their study, they used a thermophilic archaeal AcP from *Sulfolobus solfataricus* (SsoAcp), which allows aggregation to occur while the native structure is maintained. However, it is premature to suggest that the dimer observed in PhAcP is the precursor for the formation of nativelike aggregates in SsoAcp, because amyloid formation is sensitive to small structural modification such as single-residue substitution and PhAcP shares only 40% sequence identity to SsoAcP (Figure 1). Moreover, it is unclear how the dimer of PhAcP resembles the "nativelike" states proposed by Chiti et al. Nevertheless, the structure of PhAcP reported here provides a structural model of how two monomers of PhAcP dimerize via association of two antiparallel strands.

ACKNOWLEDGMENT

We thank Ms. Christine Tung and Lai-On Chu for technical assistance in the enzymatic assay. Generous support of Professor Alan Fersht during K.B.W.'s sabbatical visit to Cambridge is acknowledged. We also express our thanks for the critical comments made by the anonymous reviewers of this manuscript.

SUPPORTING INFORMATION AVAILABLE

The coordinates of the model of the PhAcP−acetyl phosphate complex with the lowest docking energy. This material is available free of charge via the Internet at http://pubs.acs.org.

REFERENCES

1. Stefani, M., Taddei, N., and Ramponi, G. (1997) Insights into acylphosphatase structure and catalytic mechanism, *Cell Mol. Life Sci. 53*, 141−151.
2. Paoli, P., Camici, G., Manao, G., Giannoni, E., and Ramponi, G. (2000) Acylphosphatase possesses nucleoside triphosphatase and nucleoside diphosphatase activities, *Biochem. J. 349*, 43−49.
3. Harary, I. (1957) The hydrolysis of 1,3-diphosphoglyceric acid by acyl phosphatase, *Biochim. Biophys. Acta 26*, 434−436.
4. Ramponi, G., Liguri, G., Nediani, C., Stefani, M., Taddei, N., and Nassi, P. (1988) Acylphosphatase increases the rate of ethanol production from glucose in cell-free extracts of *Saccharomyces cerevisiae*, *Biotechnol. Appl. Biochem. 10*, 408−413.
5. Raugei, G., Modesti, A., Magherini, F., Marzocchini, R., Vecchi, M., and Ramponi, G. (1996) Expression of acylphosphatase in *Saccharomyces cerevisiae* enhances ethanol fermentation rate, *Biotechnol. Appl. Biochem. 23*, 273−278.
6. Dan'shina, P. V., Schmalhausen, E. V., Arutiunov, D. Y., Pleten, A. P., and Muronetz, V. I. (2003) Acceleration of glycolysis in the presence of the non-phosphorylating and the oxidized phosphorylating glyceraldehyde-3-phosphate dehydrogenases, *Biochemistry (Moscow) 68*, 593−600.
7. Nassi, P., Nediani, C., Liguri, G., Taddei, N., and Ramponi, G. (1991) Effects of acylphosphatase on the activity of erythrocyte membrane Ca^{2+} pump, *J. Biol. Chem. 266*, 10867−10871.
8. Nediani, C., Fiorillo, C., Marchetti, E., Bandinelli, R., Degl'Innocenti, D., and Nassi, P. (1995) Acylphosphatase: A potential modulator of heart sarcolemma Na^+,K^+ pump, *Biochemistry 34*, 6668−6674.
9. Nediani, C., Fiorillo, C., Marchetti, E., Pacini, A., Liguri, G., and Nassi, P. (1996) Stimulation of cardiac sarcoplasmic reticulum calcium pump by acylphosphatase. Relationship to phospholamban phosphorylation, *J. Biol. Chem. 271*, 19066−19073.
10. Nediani, C., Fiorillo, C., Rigacci, S., Magherini, F., Francalanci, M., Liguri, G., Pacini, A., and Nassi, P. (1999) A novel interaction mechanism accounting for different acylphosphatase effects on cardiac and fast twitch skeletal muscle sarcoplasmic reticulum calcium pumps, *FEBS Lett. 443*, 308−312.
11. Nediani, C., Celli, A., Fiorillo, C., Ponziani, V., Giannini, L., and Nassi, P. (2003) Acylphosphatase interferes with SERCA2a-PLN association, *Biochem. Biophys. Res. Commun. 301*, 948−951.
12. Degl'Innocenti, D., Ramazzotti, M., Marzocchini, R., Chiti, F., Raugei, G., and Ramponi, G. (2003) Characterization of a novel *Drosophila melanogaster* acylphosphatase, *FEBS Lett. 535*, 171−174.
13. Pieri, A., Magherini, F., Liguri, G., Raugei, G., Taddei, N., Bozzetti, M. P., Cecchi, C., and Ramponi, G. (1998) *Drosophila melanogaster* acylphosphatase: A common ancestor for acylphosphatase isoenzymes of vertebrate species, *FEBS Lett. 433*, 205−210.
14. Pazzagli, L., Manao, G., Cappugi, G., Caselli, A., Camici, G., Moneti, G., and Ramponi, G. (1998) The amino acid sequences of two acylphosphatase isoforms from fish muscle (*Lamna nasus*), *Biochim. Biophys. Acta 1387*, 264−274.
15. Pastore, A., Saudek, V., Ramponi, G., and Williams, R. J. (1992) Three-dimensional structure of acylphosphatase. Refinement and structure analysis, *J. Mol. Biol. 224*, 427−440.
16. Thunnissen, M. M., Taddei, N., Liguri, G., Ramponi, G., and Nordlund, P. (1997) Crystal structure of common type acylphosphatase from bovine testis, *Structure 5*, 69−79.

17. Zuccotti, S., Rosano, C., Ramazzotti, M., Degl'Innocenti, D., Stefani, M., Manao, G., and Bolognesi, M. (2004) Three-dimensional structural characterization of a novel *Drosophila melanogaster* acylphosphatase, *Acta Crystallogr., Sect. D 60*, 1177−1179.
18. Gonzalez, J. M., Masuchi, Y., Robb, F. T., Ammerman, J. W., Maeder, D. L., Yanagibayashi, M., Tamaoka, J., and Kato, C. (1998) *Pyrococcus horikoshii* sp. nov., a hyperthermophilic archaeon isolated from a hydrothermal vent at the Okinawa Trough, *Extremophiles 2*, 123−130.
19. Cheung, Y. Y., Allen, M. D., Bycroft, M., and Wong, K. B. (2004) Crystallization and preliminary crystallographic analysis of an acylphosphatase from the hyperthermophilic archaeon *Pyrococcus horikoshii*, *Acta Crystallogr., Sect. D 60*, 1308−1310.
20. Collaborative Computational Project Number 4 (1994) The CCP4 suite: Programs for protein crystallography, *Acta Crystallogr., Sect. D 50*, 760−763.
21. Vagin, A. A., and Isupov, M. N. (2001) Spherically averaged phased translation function and its application to the search for molecules and fragments in electron-density maps, *Acta Crystallogr., Sect. D 57*, 1451−1456.
22. Brunger, A. T., Adams, P. D., Clore, G. M., DeLano, W. L., Gros, P., Grosse-Kunstleve, R. W., Jiang, J. S., Kuszewski, J., Nilges, M., Pannu, N. S., Read, R. J., Rice, L. M., Simonson, T., and Warren, G. L. (1998) Crystallography and NMR system: A new software suite for macromolecular structure determination, *Acta Crystallogr., Sect. D 54*, 905−921.
23. McRee, D. E. (1999) XtalView/Xfit−A versatile program for manipulating atomic coordinates and electron density, *J. Struct. Biol. 125*, 156−165.
24. Read, R. (1987) Improved Fourier coefficients for maps using phases from partial structures with errors, *Acta Crystallogr., Sect. A 42*, 140−149.
25. Murshudov, G. N. (1997) Refinement of macromolecular structures by the maximum-likelihood method, *Acta Crystallogr., Sect. D 53*, 240−255.
26. Laskowski, R. A., MacArthur, M. W., Moss, D. S., and Thornton, J. M. (1993) PROCHECK: A program to check the stereochemical quality of protein structures, *J. Appl. Crystallogr. 26*, 283−291.
27. Ramponi, G., Treves, C., and Guerritore, A. (1966) Continuous optical assay of acylphosphatase with benzoylphosphate as substrate, *Experientia 22*, 705−706.
28. Camici, G., Cappugi, G., and Ramponi, G. (1976) A new synthesis of benzoyl phosphate: A substrate for acyl phosphate assay, *Experientia 32*, 535−536.
29. Pace, C. N., and Scholtz, J. M. (1997) in *Protein Structure* (Creighton, T. E., Ed.) pp 299, Oxford University Press, Oxford, U.K.
30. Santoro, M. M., and Bolen, D. W. (1988) Unfolding free energy changes determined by the linear extrapolation method. 1. Unfolding of phenylmethanesulfonyl α-chymotrypsin using different denaturants, *Biochemistry 27*, 8063−8068.
31. Morris, G. M., Goodsell, D. S., Halliday, R. S., Huey, R., Hart, W. E., Belew, R. K., and Olson, A. J. (1988) Automated docking using a Lamarckian genetic algorithm and empirical binding free energy function, *J. Comput. Chem. 19*, 1639−1662.
32. Schuttelkopf, A. W., and van Aalten, D. M. (2004) PRODRG: A tool for high-throughput crystallography of protein−ligand complexes, *Acta Crystallogr., Sect. D 60*, 1355−1363.
33. Kawarabayasi, Y., Sawada, M., Horikawa, H., Haikawa, Y., Hino, Y., Yamamoto, S., Sekine, M., Baba, S., Kosugi, H., Hosoyama, A., Nagai, Y., Sakai, M., Ogura, K., Otsuka, R., Nakazawa, H., Takamiya, M., Ohfuku, Y., Funahashi, T., Tanaka, T., Kudoh, Y., Yamazaki, J., Kushida, N., Oguchi, A., Aoki, K., and Kikuchi, H. (1998) Complete sequence and gene organization of the genome of a hyper-thermophilic archaebacterium, *Pyrococcus horikoshii* OT3, *DNA Res. 5*, 55−76.
34. Taddei, N., Chiti, F., Paoli, P., Fiaschi, T., Bucciantini, M., Stefani, M., Dobson, C. M., and Ramponi, G. (1999) Thermodynamics and kinetics of folding of common-type acylphosphatase: Comparison to the highly homologous muscle isoenzyme, *Biochemistry 38*, 2135−2142.
35. Chiti, F., van Nuland, N. A., Taddei, N., Magherini, F., Stefani, M., Ramponi, G., and Dobson, C. M. (1998) Conformational stability of muscle acylphosphatase: The role of temperature, denaturant concentration, and pH, *Biochemistry 37*, 1447−1455.
36. Taddei, N., Stefani, M., Vecchi, M., Modesti, A., Raugei, G., Bucciantini, M., Magherini, F., and Ramponi, G. (1994) Arginine-23 is involved in the catalytic site of muscle acylphosphatase, *Biochim. Biophys. Acta 1208*, 75−80.
37. Taddei, N., Stefani, M., Magherini, F., Chiti, F., Modesti, A., Raugei, G., and Ramponi, G. (1996) Looking for residues involved in the muscle acylphosphatase catalytic mechanism and structural stabilization: Role of Asn41, Thr42, and Thr46, *Biochemistry 35*, 7077−7083.
38. Rosano, C., Zuccotti, S., Bucciantini, M., Stefani, M., Ramponi, G., and Bolognesi, M. (2002) Crystal structure and anion binding in the prokaryotic hydrogenase maturation factor HypF acylphosphatase-like domain, *J. Mol. Biol. 321*, 785−796.
39. Hengge, A. C. (1998) in *Comprehensive Biological Catalysis. A Mechanistic Reference* (Sinnott, M., Ed.) pp 517−542, Academic Press, London, U.K.
40. Paoli, P., Cirri, P., Camici, L., Manao, G., Cappugi, G., Moneti, G., Pieraccini, G., Camici, G., and Ramponi, G. (1997) Common-type acylphosphatase: Steady-state kinetics and leaving-group dependence, *Biochem. J. 327*, 177−184.
41. Jaenicke, R., and Bohm, G. (2001) Thermostability of proteins from *Thermotoga maritima*, *Methods Enzymol. 334*, 438−469.
42. Szilagyi, A., and Zavodszky, P. (2000) Structural differences between mesophilic, moderately thermophilic, and extremely thermophilic protein subunits: Results of a comprehensive survey, *Structure Fold Des. 8*, 493−504.
43. Kumar, S., Tsai, C. J., and Nussinov, R. (2000) Factors enhancing protein thermostability, *Protein Eng. 13*, 179−191.
44. Vogt, G., Woell, S., and Argos, P. (1997) Protein thermal stability, hydrogen bonds, and ion pairs, *J. Mol. Biol. 269*, 631−643.
45. Vogt, G., and Argos, P. (1997) Protein thermal stability: Hydrogen bonds or internal packing? *Fold Des. 2*, S40−S46.
46. Querol, E., Perez-Pons, J. A., and Mozo-Villarias, A. (1996) Analysis of protein conformational characteristics related to thermostability, *Protein Eng. 9*, 265−271.
47. Petsko, G. A. (2001) Structural basis of thermostability in hyperthermophilic proteins, or "there's more than one way to skin a cat", *Methods Enzymol. 334*, 469−478.
48. Hendsch, Z. S., and Tidor, B. (1994) Do salt bridges stabilize proteins? A continuum electrostatic analysis, *Protein Sci. 3*, 211−226.
49. Elcock, A. H. (1998) The stability of salt bridges at high temperatures: Implications for hyperthermophilic proteins, *J. Mol. Biol. 284*, 489−502.
50. Makhatadze, G. I., Loladze, V. V., Gribenko, A. V., and Lopez, M. M. (2004) Mechanism of thermostabilization in a designed cold shock protein with optimized surface electrostatic interactions, *J. Mol. Biol. 336*, 929−942.
51. Makhatadze, G. I., Loladze, V. V., Ermolenko, D. N., Chen, X., and Thomas, S. T. (2003) Contribution of surface salt bridges to protein stability: Guidelines for protein engineering, *J. Mol. Biol. 327*, 1135−1148.
52. Perl, D., and Schmid, F. X. (2001) Electrostatic stabilization of a thermophilic cold shock protein, *J. Mol. Biol. 313*, 343−357.
53. Spector, S., Wang, M., Carp, S. A., Robblee, J., Hendsch, Z. S., Fairman, R., Tidor, B., and Raleigh, D. P. (2000) Rational modification of protein stability by the mutation of charged surface residues, *Biochemistry 39*, 872−879.
54. Perl, D., Mueller, U., Heinemann, U., and Schmid, F. X. (2000) Two exposed amino acid residues confer thermostability on a cold shock protein, *Nat. Struct. Biol. 7*, 380−383.
55. Loladze, V. V., Ibarra-Molero, B., Sanchez-Ruiz, J. M., and Makhatadze, G. I. (1999) Engineering a thermostable protein via optimization of charge−charge interactions on the protein surface, *Biochemistry 38*, 16419−16423.
56. Ibarra-Molero, B., Loladze, V. V., Makhatadze, G. I., and Sanchez-Ruiz, J. M. (1999) Thermal versus guanidine-induced unfolding of ubiquitin. An analysis in terms of the contributions from charge−charge interactions to protein stability, *Biochemistry 38*, 8138−8149.
57. Grimsley, G. R., Shaw, K. L., Fee, L. R., Alston, R. W., Huyghues-Despointes, B. M., Thurlkill, R. L., Scholtz, J. M., and Pace, C. N. (1999) Increasing protein stability by altering long-range Coulombic interactions, *Protein Sci. 8*, 1843−1849.
58. Matthews, B. W., Nicholson, H., and Becktel, W. J. (1987) Enhanced protein thermostability from site-directed mutations that decrease the entropy of unfolding, *Proc. Natl. Acad. Sci. U.S.A. 84*, 6663−6667.
59. Georlette, D., Damien, B., Blaise, V., Depiereux, E., Uversky, V. N., Gerday, C., and Feller, G. (2003) Structural and functional

adaptations to extreme temperatures in psychrophilic, mesophilic, and thermophilic DNA ligases, *J. Biol. Chem. 278*, 37015−37023.
60. Collins, T., Meuwis, M. A., Gerday, C., and Feller, G. (2003) Activity, stability, and flexibility in glycosidases adapted to extreme thermal environments, *J. Mol. Biol. 328*, 419−428.
61. D'Amico, S., Marx, J. C., Gerday, C., and Feller, G. (2003) Activity−stability relationships in extremophilic enzymes, *J. Biol. Chem. 278*, 7891−7896.
62. Fitter, J., Herrmann, R., Dencher, N. A., Blume, A., and Hauss, T. (2001) Activity and stability of a thermostable α-amylase compared to its mesophilic homologue: Mechanisms of thermal adaptation, *Biochemistry 40*, 10723−10731.
63. Svingor, A., Kardos, J., Hajdu, I., Nemeth, A., and Zavodszky, P. (2001) A better enzyme to cope with cold. Comparative flexibility studies on psychrotrophic, mesophilic, and thermophilic IPMDHs, *J. Biol. Chem. 276*, 28121−28125.
64. Chiti, F., Calamai, M., Taddei, N., Stefani, M., Ramponi, G., and Dobson, C. M. (2002) Studies of the aggregation of mutant proteins *in vitro* provide insights into the genetics of amyloid diseases, *Proc. Natl. Acad. Sci. U.S.A. 99*, 16419−16426.
65. Chiti, F., Stefani, M., Taddei, N., Ramponi, G., and Dobson, C. M. (2003) Rationalization of the effects of mutations on peptide and protein aggregation rates, *Nature 424*, 805−808.
66. Chiti, F., Taddei, N., Stefani, M., Dobson, C. M., and Ramponi, G. (2001) Reduction of the amyloidogenicity of a protein by specific binding of ligands to the native conformation, *Protein Sci. 10*, 879−886.
67. Chiti, F., Taddei, N., Webster, P., Hamada, D., Fiaschi, T., Ramponi, G., and Dobson, C. M. (1999) Acceleration of the folding of acylphosphatase by stabilization of local secondary structure, *Nat. Struct. Biol. 6*, 380−387.
68. Taddei, N., Capanni, C., Chiti, F., Stefani, M., Dobson, C. M., and Ramponi, G. (2001) Folding and aggregation are selectively influenced by the conformational preferences of the α-helices of muscle acylphosphatase, *J. Biol. Chem. 276*, 37149−37154.
69. Taddei, N., Chiti, F., Fiaschi, T., Bucciantini, M., Capanni, C., Stefani, M., Serrano, L., Dobson, C. M., and Ramponi, G. (2000) Stabilisation of α-helices by site-directed mutagenesis reveals the importance of secondary structure in the transition state for acylphosphatase folding, *J. Mol. Biol. 300*, 633−647.
70. Monti, M., Garolla di Bard, B. L., Calloni, G., Chiti, F., Amoresano, A., Ramponi, G., and Pucci, P. (2004) The regions of the sequence most exposed to the solvent within the amyloidogenic state of a protein initiate the aggregation process, *J. Mol. Biol. 336*, 253−262.
71. Chiti, F., Webster, P., Taddei, N., Clark, A., Stefani, M., Ramponi, G., and Dobson, C. M. (1999) Designing conditions for *in vitro* formation of amyloid protofilaments and fibrils, *Proc. Natl. Acad. Sci. U.S.A. 96*, 3590−3594.
72. Plakoutsi, G., Taddei, N., Stefani, M., and Chiti, F. (2004) Aggregation of the acylphosphatase from *Sulfolobus solfataricus*: The folded and partially unfolded states can both be precursors for amyloid formation, *J. Biol. Chem. 279*, 14111−14119.
73. McDonald, I. K., and Thornton, J. M. (1994) Satisfying hydrogen bonding potential in proteins, *J. Mol. Biol. 238*, 777−793.
74. Hubbard, S. J., Campbell, S. F., and Thornton, J. M. (1991) Molecular recognition. Conformational analysis of limited proteolytic sites and serine proteinase protein inhibitors, *J. Mol. Biol. 220*, 507−530.
75. Thompson, J. D., Higgins, D. G., and Gibson, T. J. (1994) CLUSTAL W: Improving the sensitivity of progressive multiple sequence alignment through sequence weighting, position-specific gap penalties, and weight matrix choice, *Nucleic Acids Res. 22*, 4673−4680.

BI047832K